ARTICLE

In situ Investigations of Interfacial Degradation and Ion Migration at $CH_3NH_3PbI_3$ Perovskite/Ag Interfaces

Xiong Li[a†], Hong-he Ding[a†], Gui-hang Li[a], Yan Wang[a], Zhi-min Fang[b], Shang-feng Yang[b], Huan-xin Ju[a], Jun-fa Zhu[a*]

a. National Synchrotron Radiation Laboratory and Department of Chemical Physics, University of Science and Technology of China, Hefei 230029, China
b. Hefei National Laboratory for Physical Sciences at the Microscale, Key Laboratory of Materials for Energy Conversion, Chinese Academy of Sciences, Department of Materials Science and Engineering, Synergetic Innovation Center of Quantum Information & Quantum Physics, University of Science and Technology of China, Hefei 230026, China

(Dated: Received on August 19, 2018; Accepted on September 18, 2018)

Interfacial properties between perovskite layers and metal electrodes play a crucial role in the device performance and the long-term stability of perovskite solar cells. Here, we report a comprehensive study of the interfacial degradation and ion migration at the interface between $CH_3NH_3PbI_3$ perovskite layer and Ag electrode. Using *in situ* photoemission spectroscopy measurements, we found that the Ag electrode could induce the degradation of perovskite layers, leading to the formation of PbI_2 and AgI species and the reduction of Pb^{2+} ions to metallic Pb species at the interface. The unconventional enhancement of the intensities of I 3d spectra provides direct experimental evidences for the migration of iodide ions from $CH_3NH_3PbI_3$ subsurface to Ag electrode. Moreover, the contact of Ag electrode and perovskite layers induces an interfacial dipole of 0.3 eV at $CH_3NH_3PbI_3$/Ag interfaces, which may further facilitate iodide ion diffusion, resulting in the decomposition of perovskite layers and the corrosion of Ag electrode.

Key words: Perovskite solar cells, Interfacial degradation, Ions migration, Photoemission spectroscopy

I. INTRODUCTION

Perovskite solar cells are considered as one of the most promising candidates for the next generation photovoltaic technology due to the high power conversion efficiency (over 22.7%) and low cost fabrication [1, 2]. However, despite these advantages, the long-term stability issues inhibit the further commercial development [3, 4]. In order to address these issues, numerous research efforts have been made to understand the degradation mechanisms caused by the halide perovskite itself and charge transport materials as well as interfaces of the devices [5–8]. The inorganic-organic hybrid halide perovskite materials are extremely sensitive to environmental conditions, such as moisture, temperature, ultraviolet irradiation, and oxygen atmosphere [9–11]. However, considerable degradation of perovskite solar cells was still observed even when the encapsulation techniques were applied to perovskite solar cells to avoid these environmental factors [12–14]. These results indicate that the environmental effects are not the only crucial factors determining device stability, but the intrinsic factors also facilitate the degradation. Therefore, it is necessary to understand the role of interfaces in stability of perovskite solar cells to achieve highly stable devices.

Typically, perovskite solar cells have a sandwich structure. The top electrode, as one of the most essential components, has a direct impact on the device performance and long-term stability [15–17]. Silver (Ag) is one of the most commonly used electrode materials in p-i-n perovskite solar cells due to the low-cost and favorable energy level alignment compared to Au electrode. Recent studies have demonstrated that the reactivity between the metal electrode and perovskite is the main degradation route, which directly influences the chemical stability of the devices [18–20]. Han *et al.*, for example, studied degradation of encapsulated planar $CH_3NH_3PbI_3$ perovskite solar cells with the Ag back-contact electrode layer using scanning electron microscopy (SEM) and X-ray diffraction (XRD). They observed the corrosion of Ag electrode and appearance of PbI_2 and AgI species under the conditions of high temperature and humidity [14]. Kato *et al.* also studied the corrosion of Ag electrode on $CH_3NH_3PbI_3$/spiro-

†These authors contributed equally to this work.
*Author to whom correspondence should be addressed.
E-mail: jfzhu@ustc.edu.cn

MeOTAD by XRD and X-ray photoelectron spectroscopy (XPS). They claimed that Ag electrode was corroded to produce AgI species owing to the migration of methyl ammonium iodide through the spiro-MeOTAD layer under the assistance of H_2O in air [21]. In addition, Li *et al.* used time-of-flight secondary ion mass spectroscopy (TOF-SIMS) to investigate the thermal stability process of perovskite devices with Ag electrode. They have shown that the I^- ions from the $CH_3NH_3PbI_3$ layer diffused through the PCBM to the Ag back-contact surface and demonstrated that the thermal degradation was induced by Ag electrode [22]. All these studies emphasize the importance of interfacial interaction and ion migration between perovskite layers and Ag electrode. However, due to the relatively low activation barrier (0.1 eV) of iodide migration [23–25], the iodide ions migration can be easily changed by external environmental factors (*e.g.* moisture or temperature) [21, 22]. It is still unclear how the Ag electrode induces the interfacial interaction with perovskite layers in the absence of the external environmental factors. Therefore, an *in-situ* study on the reaction of the Ag internal interfaces is essential to the understanding of the exact origin of stability issues.

In this work, we focus on the effects of the interfacial structures of Ag electrode with the perovskite layers on the degradation of perovskite layers. The corrosion of Ag electrode and the decomposition of perovskite layers were *in situ* investigated by high resolution synchrotron radiation photoemission spectroscopy (SRPES) and XPS. The PbI_2 and AgI species at the $CH_3NH_3PbI_3$/Ag interface are identified by XRD and XPS, respectively. The migration of iodide ions towards Ag electrode is directly confirmed by the anomalous enhancement of I 3d XP spectra intensity, which is possibly facilitated by an interfacial dipole of 0.3 eV at the $CH_3NH_3PbI_3$/Ag interface.

II. EXPERIMENTS

$CH_3NH_3PbI_3$ layers were fabricated in a glove box, as described in a previous report [26]. Briefly, the precursors were prepared with 1 mmol CH_3NH_3I and 1 mmol PbI_2, dissolved in 1 mL mixed solvent of dimethyl formamide (DMF):dimethylsulfoxide (DMSO) (7:3, V/V). The mixture was stirred in the glove box at 60 °C overnight, then filtered with a 0.45 μm filter, and finally spin-coated onto the indium tin oxide (ITO)/NiO substrates at 4000 r/min for 20 s. In addition, 70 μL chlorobenzene was added dropwise onto the substrates, in order to wipe off the redundant solvent. The ITO/NiO/$CH_3NH_3PbI_3$ samples were annealed at 100 °C for 10 min, and subsequently transferred to the ultra-high vacuum (UHV) chamber with a base pressure larger than 2×10^{-10} mbar for analysis. The deposition of Ag metal (99.999%, Alfa Aesar) on the $CH_3NH_3PbI_3$ surface was carried out in a molecular beam epitaxy (MBE) chamber at 3×10^{-9} mbar. There is no report about the sticking probability of Ag on the $CH_3NH_3PbI_3$ surface, thus the thickness of the evaporated silver was defined by a quartz crystal microbalance (QCM).

The SRPES and XPS experiments were performed at the Catalysis and Surface Science Endstation at the BL11U beamline of National Synchrotron Radiation Laboratory (NSRL), Hefei, China. The detailed description of the beamline and endstation can be found elsewhere [27]. The core levels of Ag 3d, N 1s, C 1s, and Pb 4f spectra were measured *in situ* immediately after each metal deposition with photon energies of 480 eV, 400 eV, and 200 eV, respectively, which were calibrated using the bulk Au $4f_{7/2}$ core level located at 84.0 eV as the reference. The valence-band spectra were measured with a photon energy of 40 eV and referenced to the Fermi level determined from a bulklike Ag layer on the sample. A sample bias of −5.0 V was applied in order to observe the secondary electron cut-off. The peak fitting was performed by using the XPS Peak 41 program with Gaussian functions after subtraction of the linear background. XRD patterns of the samples (before and after Ag deposition) were recorded on a Rigaku Miniflex-600 operating at 40 kV voltage and 15 mA current with Cu Kα radiation (λ=0.15406 nm).

III. RESULTS AND DISCUSSION

FIG. 1(a) presents the XPS survey spectrum of the pristine $CH_3NH_3PbI_3$ layer (red curve), the peak assignments are in good agreement with the elemental compositions of the $CH_3NH_3PbI_3$ layer. After depositing 64 Åthick Ag on the $CH_3NH_3PbI_3$ surface, the Ag 3d peak shows up in the XPS survey spectrum (blue curve). In addition, no O 1s signal is observed, indicating that the degradation of perovskite layers induced by residual oxygen or moisture does not happen during the measurements. Moreover, after 64 Å Ag deposition, the Pb 4f signal is still obvious and the Ag 3d signal is not very strong, which may be relative to the low condensation coefficient of Ag on $CH_3NH_3PbI_3$ surface at elevated temperature, just like Ag evaporating on the polymer surface [28, 29]. In order to prove this speculation, the parallel controlled experiments were performed by depositing Ag on $CH_3NH_3PbI_3$ surface at various temperatures (100, 200, and 300 K), and got surface sensitive information by changing the detection angles. The results are shown in FIG. S1 (supplementary materials). Obviously, the Ag 3d signal at 100 K is much stronger than that at 300 K, indicating that the condensation coefficient of Ag at 300 K is much lower than that of Ag at 100 K. In addition, at the same thickness and temperature, the Ag 3d signal collected at grazing emission (θ=60°, with respect to the surface normal) is much stronger than that at the normal emission (θ=0°), as shown in FIG. S2 in supplemen-

DOI:10.1063/1674-0068/cjcp1808189

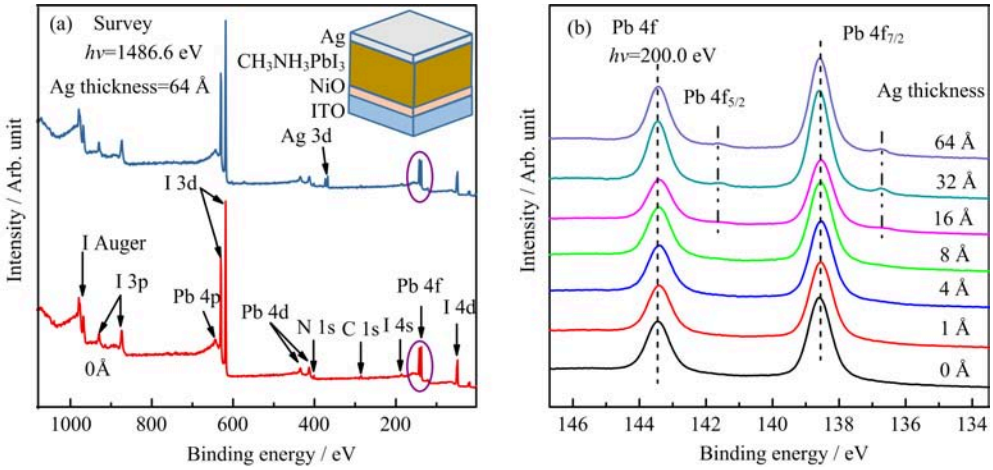

FIG. 1 (a) XPS survey spectra of the pristine $CH_3NH_3PbI_3$ layer (red curve) and the sample deposited with 64 Å of Ag (blue curve). The inset shows the schematic architecture of the sample ITO/NiO/$CH_3NH_3PbI_3$/Ag. (b) The evolution of Pb 4f XPS as a function of the Ag thickness.

tary materials, which suggests that Ag atoms mainly distribute on the $CH_3NH_3PbI_3$ surface, and just small part of Ag atoms diffuse downward.

In order to get further insights into the interfacial interaction, the evolution of the Pb 4f spectra as a function of Ag thickness was monitored, as presented in FIG. 1(b). For the pristine perovskite layers, the Pb $4f_{7/2}$ spectra only present one component at 138.6 eV, which is attributed to Pb^{2+} ions in the $CH_3NH_3PbI_3$ layer [30]. With increasing Ag thickness, a new small peak appears at the lower binding energy side and becomes more remarkable after 32 Å thick Ag was deposited. This new peak at 136.7 eV is assigned to metallic Pb species [30]. This result indicates the chemical reaction of Ag electrode with perovskite layers. However, it should be noted that the thermal radiation from the evaporator may also cause the degradation of perovskite layer to form metallic Pb species [31]. In order to exclude this possibility, a parallel experiment was carried out by placing a pristine sample at the same evaporation position with the empty evaporator. After the sample was thermally irradiated at the same evaporation temperature (740 °C) for 1 h, no obvious changes can be observed in Pb 4f spectrum compared to that before the thermal radiation (see FIG. S3 in supplementary materials). This suggests that the appearance of metallic Pb caused by thermal radiation can be excluded. Therefore, it is concluded that the metallic Pb species originates from the interfacial interaction between Ag electrode and $CH_3NH_3PbI_3$ layers.

The XRD experiments were also performed for the samples before and after Ag deposition. The results are shown in FIG. 2. For the pristine sample, the XRD pattern shows peaks at 2θ=14.37°, 20.29°, 23.71°, 24.74°, 28.72°, 32.14°, and 40.91°. They can be attributed to the (110), (200), (211), (202), (220), (310), and (224) planes of the tetragonal structured $CH_3NH_3PbI_3$ crys-

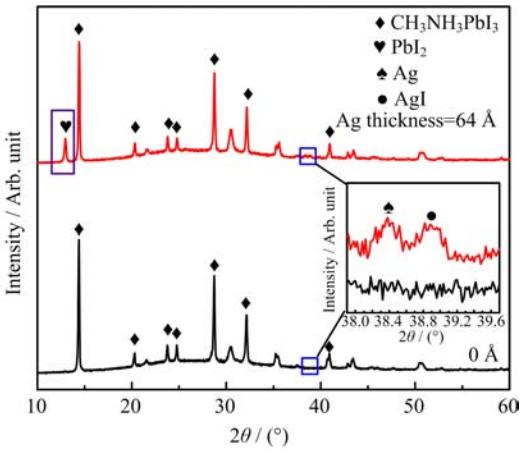

FIG. 2 The XRD patterns of the pristine $CH_3NH_3PbI_3$ sample and the sample deposited with 64 Åthick Ag. The inset is the partialy enlarged view of the XRD pattern (from 37.9° to 39.7°). The characteristic peaks at 2θ=38.35° and 38.95° correspond to metallic Ag and AgI species, respectively. The peak at 2θ=12.89° corresponds to PbI_2 species.

tal, respectively [32, 33]. After 64 Å thick Ag is deposited, a new peak appears at 2θ=12.89°, which can be assigned to (001) plane of PbI_2 phase [34]. In addition, from the partially enlarged XRD pattern (inset of FIG. 2), two small peaks at 2θ=38.35° and 38.95°, attributed to the Ag and AgI species, respectively [21], can be observed. Therefore, the XRD results further confirm the occurrence of the decomposition of $CH_3NH_3PbI_3$ layers induced by Ag electrode deposition and formation of AgI and PbI_2 phase.

FIG. 3 (a) and (b) show the evolution of Ag 3d and I 3d core-level spectra for different thickness of Ag onto the $CH_3NH_3PbI_3$ layer, respectively. As shown in FIG. 3(a), with increasing the Ag thickness, the shift

DOI:10.1063/1674-0068/cjcp1808189

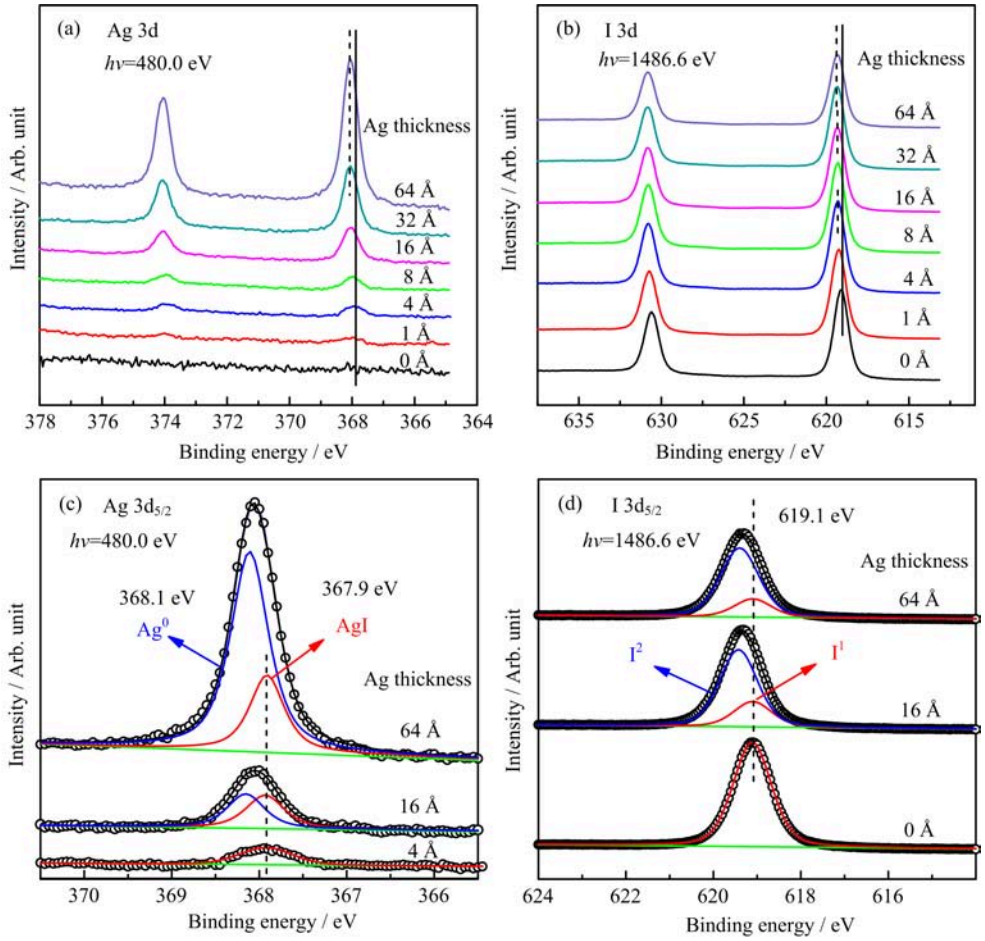

FIG. 3 The evolution of (a) Ag 3d, (b) I 3d core-level spectra as a function of the Ag thickness. Representative peak fitting results of (c) Ag $3d_{5/2}$ and (d) I $3d_{5/2}$ for Ag deposition on perovskite surface with different thicknesses.

of the peak position of Ag $3d_{5/2}$ is observed. The initial peak position of Ag $3d_{5/2}$ locates at 367.9 eV when the thickness of Ag is below 8 Å, and the peak position shifts towards higher binding energy with further increasing Ag thickness. As the Ag thickness increases up to 64 Å, the peak position of Ag $3d_{5/2}$ shifts to 368.1 eV. I 3d spectra shown in FIG. 3(b) have similar changes: the initial I $3d_{5/2}$ peak locates at 619.1 eV and then also shifts towards higher binding energy with increasing Ag thickness. After 64 Å thick Ag is deposited, the peak position of I $3d_{5/2}$ shifts to 619.4 eV. For both of the Ag $3d_{5/2}$ and I $3d_{5/2}$ spectra, the spectral line shapes are slightly broadened with increasing the Ag thickness, indicating the new species forms at the $CH_3NH_3PbI_3$/Ag interface.

In order to illuminate the detailed interfacial interactions, the deconvolution of spectra was carried out for Ag $3d_{5/2}$ and I $3d_{5/2}$ spectra, respectively. According to the previous reports, the Ag^+ state locates at the lower binding energy than the Ag^0 state, due to the impact of extra-atomic relaxation and lattice potential [35, 36]. As shown in FIG. 3(c), after 4 Å thick Ag deposition, the Ag $3d_{5/2}$ peak locates at 367.9 eV, which is attributed to Ag^+ state (labelled "AgI"). With further depositing Ag on the $CH_3NH_3PbI_3$ layers, the Ag $3d_{5/2}$ spectra can be decomposed into two components with a second peak at 368.1 eV, which is assigned to metallic Ag species (labelled "Ag^0"). Furthermore, this metallic Ag component becomes dominated species when the Ag thickness is above 16 Å. The peak-fitting result from the sample deposited with 64 Å thick Ag is fully consistent with the appearance of Ag and AgI signal in the XRD pattern. FIG. 3(d) displays the peak-fitting results of I $3d_{5/2}$ XPS spectra. For the pristine $CH_3NH_3PbI_3$ layers, the iodide ions peak (labelled "I^1") locates at 619.1 eV, which is in good agreement with that reported in Ref.[21]. After Ag deposition, a new peak (labelled "I^2") appears at the higher binding energy side (619.4 eV) with its intensity gradually increases. Because the electronegativity of Ag is smaller than that of Pb, the I^2 component can be attributed to the AgI component [35, 37]. The observations of I $3d_{5/2}$ spectra are completely consistent with the results of Ag $3d_{5/2}$ spectra.

We further analyzed the evolution of the integrated

DOI:10.1063/1674-0068/cjcp1808189

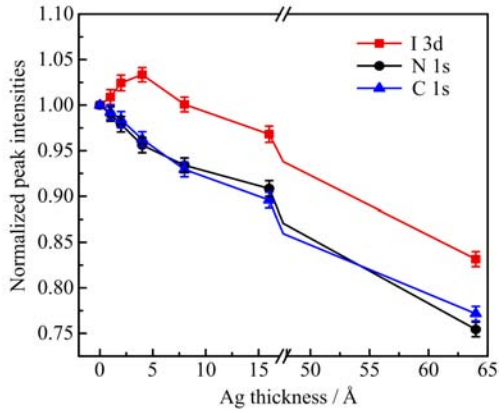

FIG. 4 The evolution of peak intensities of C 1s, N 1s, and I 3d spectra as a function of Ag thickness on the $CH_3NH_3PbI_3$ surface. The break region of the horizontal axis is from 17 Å to 48 Å. All the peak intensities are normalized to those from the pristine $CH_3NH_3PbI_3$ surface.

intensities of C 1s, N 1s, and I 3d spectra as a function of Ag thickness on the $CH_3NH_3PbI_3$ layers. The results are shown in FIG. 4. All the peak intensities are normalized to those from the pristine $CH_3NH_3PbI_3$ surface. Upon Ag deposition, the intensities of C 1s and N 1s spectra gradually decrease with almost the same rate (C 1s and N 1s spectra are shown in FIG. S4 in supplementary materials). After 64 Å thick Ag deposition, they decrease about ∼23%. In principle, the integrated intensity of I 3d spectra should also decrease with a similar rate. However, the intensity of I 3d decreases only by 13%. Interestingly, when the Ag thickness is less than 8 Å, the integrated intensity of I 3d even increases by about 4%, while those of C 1s and N 1s decrease by 5%. This distinctive changes in the substrate element peak intensities provide a direct evidence that the iodide ions migrate from the perovskite subsurface towards Ag electrode. The *in situ* photoemission spectroscopy measurements show that the chemical reaction occurs at the interface between Ag electrode and perovskite layers, and iodide ion migration may facilitate the reaction occurrence. In previous studies, the diffusion of iodide ions was attributed to the induction by external environmental factor, such as the moisture and temperature [21, 22, 38]. However, under the ultra-high vacuum conditions in our present case, the chemical reaction and ion migration were also observed.

To better understand the driving force of the iodide ions migration, the valence band and secondary electron cut-off measurements were carried out to investigate the energy level alignment at the $CH_3NH_3PbI_3$/Ag interface. FIG. 5(a) displays the valence band and secondary electron cut-off spectra before and after Ag deposition on the $CH_3NH_3PbI_3$ surface, respectively. For the pristine sample, the highest-occupied molecular orbital (HOMO) level is approximately 1.2 eV below the Fermi level, and the work function is calculated to be 5.0 eV, similar to the reported results [39]. When the

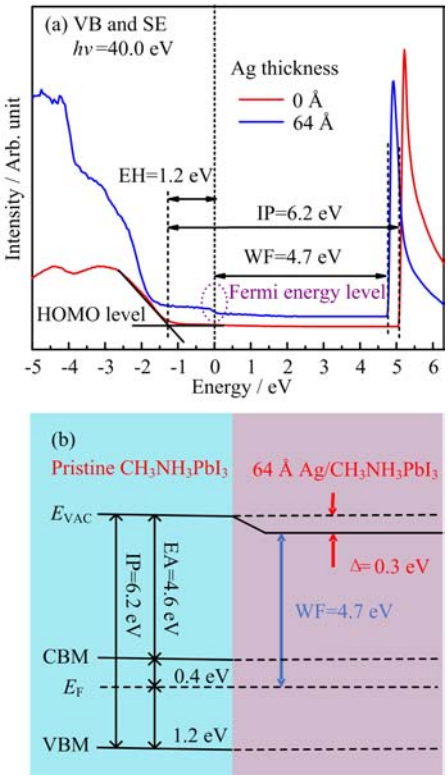

FIG. 5 (a) Thickness dependent UPS spectra of Ag on $CH_3NH_3PbI_3$ coated on the NiO/ITO substrate including the secondary cut-off region and the valence band edge region. (b) The schematic drawing of the energy level alignment diagram at the $CH_3NH_3PbI_3$/Ag interface. IP is the ionization potential, EA is the electron affinity, EH is the hole transport barrier, WF is the work function, and Δ is the interfacial dipole.

Ag thickness reaches 64 Å, the Ag Fermi energy level appears, and the work function reduces by 0.3 eV. The energy level alignment at the $CH_3NH_3PbI_3$/Ag interfaces can be derived from these results. The position of the lowest-unoccupied molecular orbital (LUMO) is determined using the reported optical band gap 1.6 eV [40] by ignoring the exciton binding energy. As shown in FIG. 5(b), a downward interfacial dipole of 0.3 eV is formed upon the contact of Ag electrode, which induces the decrease of the negative charge transport barrier from $CH_3NH_3PbI_3$ layers to Ag electrode. Since the activation barrier for iodide migration is as low as 0.1 eV [23], thus the interfacial dipole of 0.3 eV at $CH_3NH_3PbI_3$/Ag interfaces would facilitate the iodide ions migration towards Ag electrode.

According to the above experimental observations, it is concluded that the chemical reaction occurs between the Ag electrode and perovskite layers, which is an important factor that influences the perovskite stability. In particular, the direct evidence has been provided to confirm the iodide ions migration and the interfacial dipole would facilitate this migration process. The migration and accumulation of iodide ions induced two

DOI:10.1063/1674-0068/cjcp1808189

effects: the decomposition of perovskite layers and the corrosion of the Ag electrode. Nevertheless, compared with Au electrode, Ag is still a favorable electrode material with the advantages of low cost, low work function, and the appropriate energy level alignment. Therefore, in order to improve the device stability, charge transport layers should be applied between the top electrode and perovskite layers to prevent the interfacial degradation [41, 42]. Because of the pinholes in spiro-MeOTAD layer and high "solubility" of iodide ions in PCBM layer, the blocking effect of these organic materials was not obvious. In contrast, the inorganic charge transport layers, such as MoO_3 [19] and CuSCN [43], could form a compact layer to prevent the Ag atom diffusion and iodide ions migration. In addition, the interfacial dipole should be considered to help solving the stability issue induced by ion migration.

IV. CONCLUSION

In summary, *in situ* XPS and SRPES have been carried out to study the interfacial properties and the ions migration at the $CH_3NH_3PbI_3$/Ag interface. Upon Ag deposion onto the $CH_3NH_3PbI_3$ surface, Ag atoms preferentially interact with iodide ions, leading to the formation of AgI species and the reduction of Pb^{2+} to Pb^0 at the interface. The migration of iodide ions towards Ag electrode is directly confirmed by the anomalous enhancement of the intensity of the I 3d XPS. Notably, after 64 Å thick Ag deposition, the interfacial dipole of 0.3 eV between the $CH_3NH_3PbI_3$ layers and Ag electrode possibly provides one of the driving forces for the migration of iodide ions, which is detrimental for the stability of $CH_3NH_3PbI_3$ layers. Therefore, for the fabrication of perovskite solar cells, introduction of an ideal buffer layer between the metal cathode and perovskite layers which can prevent the chemical reactions but keep excellent ohmic contact between Ag electrode and $CH_3NH_3PbI_3$ active layer is needed. We expect that all the information obtained in this study will be helpful for the reasonable design of the perovskite photovoltaic devices based on Ag electrode with high performances and excellent stability.

Supplementary materials: The results of parallel controlled experiments and C 1s, N 1s spectra are shown.

V. ACKNOWLEDGEMENTS

This work was supported by the National Natural Science Foundation of China (No.21473178, No.21773222, No.21503203), the National Key R&D program of China (2017YFA0403403), the Key Program of Research and Development of Hefei Science Center of CAS (2017HSC-KPRD001) and the Collaborative Innovation Center of Suzhou Nano Science and Technology.

[1] F. Fu, S. Pisoni, T. P. Weiss, T. Feurer, A. Wäckerlin, P. Fuchs, S. Nishiwaki, L. Zortea, A. N. Tiwari, and S. Buecheler, Adv. Sci. **5**, 3 (2017).
[2] A. Kojima, K. Teshima, Y. Shirai, and T. Miyasaka, J. Am. Chem. Soc. **131**, 17 (2009).
[3] H. Zhou, Y. Shi, Q. Dong, H. Zhang, Y. Xing, K. Wang, Y. Du, and T. Ma, J. Phys. Chem. Lett. **5**, 18 (2014).
[4] F. Bella, G. Griffini, J. P. Correa-Baena, G. Saracco, M. Grätzel, A. Hagfeldt, S. Turri, and C. Gerbaldi, Science **354**, 6309 (2016).
[5] L. K. Ono and Y. Qi, J. Phys. Chem. Lett. **7**, 22 (2016).
[6] J. Shi, X. Xu, D. Li, and Q. Meng, Small **11**, 21 (2015).
[7] Z. Zhou, S. Pang, Z. Liu, H. Xu, and G. Cui, J. Mater. Chem. A **3**, 38 (2015).
[8] T. Leijtens, G. E. Eperon, N. K. Noel, S. N. Habisreutinger, A. Petrozza, and H. J. Snaith, Adv. Energy Mater. **5**, 20 (2015).
[9] G. Niu, X. Guo, and L. Wang, J. Mater. Chem. A **3**, 17 (2015).
[10] M. Shahbazi and H. Wang, Solar Energy **123**, (2016).
[11] N. Aristidou, I. Sanchez-Molina, T. Chotchuangchutchaval, M. Brown, L. Martinez, T. Rath, and S. A. Haque, Angew. Chem. **54**, 28 (2015).
[12] T. A. Berhe, W. N. Su, C. H. Chen, C. J. Pan, J. H. Cheng, H. M. Chen, M. C. Tsai, L. Y. Chen, A. A. Dubale, and B. J. Hwang, Energy Environ. Sci. **9**, 2 (2016).
[13] S. Ito, S. Tanaka, K. Manabe, and H. Nishino, J. Phys. Chem. C **118**, 30 (2014).
[14] Y. Han, S. Meyer, Y. Dkhissi, K. Weber, J. M. Pringle, U. Bach, L. Spiccia, and Y. B. Cheng, J. Mater. Chem. A **3**, 15 (2015).
[15] J. W. Xiao, C. Shi, C. Zhou, D. Zhang, Y. Li, and Q. Chen, Solar RRL **1**, 9 (2017).
[16] J. Wang, X. Chen, F. Jiang, Q. Luo, L. Zhang, M. Tan, M. Xie, Y. Q. Li, Y. Zhou, W. Su, Y. Li, and C. Q. Ma, Solar RRL **2**, 1800118 (2018).
[17] W. Ming, D. Yang, T. Li, L. Zhang, and M. H. Du, Adv. Sci. **5**, 2 (2018).
[18] K. Domanski, J. P. Correa-Baena, N. Mine, M. K. Nazeeruddin, A. Abate, M. Saliba, W. Tress, A. Hagfeldt, and M. Grätzel, ACS Nano **10**, 6 (2016).
[19] E. M. Sanehira, B. J. Tremolet de Villers, P. Schulz, M. O. Reese, S. Ferrere, K. Zhu, L. Y. Lin, J. J. Berry, and J. M. Luther, ACS Energy Lett. **1**, 1 (2016).
[20] A. Guerrero, J. You, C. Aranda, Y. S. Kang, G. Garcia-Belmonte, H. Zhou, J. Bisquert, and Y. Yang, ACS Nano **10**, 1 (2016).
[21] Y. Kato, L. K. Ono, M. V. Lee, S. Wang, S. R. Raga, and Y. Qi, Adv. Mater. Inter. **2**, 13 (2015).
[22] J. Li, Q. Dong, N. Li, and L. Wang, Adv. Energy Mater. **7**, 14 (2017).
[23] J. M. Azpiroz, E. Mosconi, J. Bisquert, and F. De Angelis, Energy Environ. Sci. **8**, 7 (2015).
[24] Y. Yuan and J. Huang, Acc. Chem. Res. **49**, 2 (2016).
[25] C. Eames, J. M. Frost, P. R. Barnes, B. C. O'Regan, A. Walsh, and M. S. Islam, Nat. Commun. **6**, 7497 (2015).

DOI:10.1063/1674-0068/cjcp1808189

[26] F. Xia, Q. Wu, P. Zhou, Y. Li, X. Chen, Q. Liu, J. Zhu, S. Dai, Y. Lu, and S. Yang, ACS Appl. Mater. Inter. **7**, 24 (2015).
[27] H. Ju, K. M. Knesting, W. Zhang, X. Pan, C. H. Wang, Y. W. Yang, D. S. Ginger, and J. Zhu, ACS Appl. Mater. Inter. **8**, 3 (2016).
[28] S. D. Gardner, C. S. K. Singamsetty, G. L. Booth, G. R. He, and C. U. Pittman Jr., Carbon **33**, 587 (1995)
[29] J. Carrillo, A. Guerrero, S. Rahimnejad, O. Almora, I. Zarazua, E. Mas-Marza, J. Bisquert, and G. Garcia-Belmonte, Adv. Energy Mater. **6**, 9 (2016).
[30] T. W. Ng, C. Y. Chan, M. F. Lo, Z. Q. Guan, and C. S. Lee, J. Mater. Chem. A **3**, 17 (2015).
[31] B. Conings, J. Drijkoningen, N. Gauquelin, A. Babayigit, J. D'Haen, L. D'Olieslaeger, A. Ethirajan, J. Verbeeck, J. Manca, E. Mosconi, F. D. Angelis, and H. G. Boyen, Adv. Energy Mater. **5**, 15 (2015).
[32] B. Wang, K. Y. Wong, S. Yang, and T. Chen, J. Mater. Chem. A **4**, 10 (2016).
[33] Q. Wu, P. Zhou, W. Zhou, X. Wei, T. Chen, and S. Yang, ACS Appl. Mater. Inter. **8**, 24 (2016).
[34] P. Luo, Z. Liu, W. Xia, C. Yuan, J. Cheng, and Y. Lu, J. Mater. Chem. A **3**, 23 (2015).
[35] C. Besleaga, L. E. Abramiuc, V. Stancu, A. G. Tomulescu, M. Sima, L. Trinca, N. Plugaru, L. Pintilie, G. A. Nemnes, M. Iliescu, H. G. Svavarsson, A. Manolescu, and I. Pintilie, J. Phys. Chem. Lett. **7**, 24 (2016).
[36] J. Lauridsen, P. Eklund, J. Lu, A. Knutsson, M. Odén, R. Mannerbro, A. M. Andersson, and L. Hultman, Tribol. Lett. **46**, 2 (2012).
[37] H. Back, G. Kim, J. Kim, J. Kong, T. K. Kim, H. Kang, H. Kim, J. Lee, S. Lee, and K. Lee, Energy Environ. Sci. **9**, 4 (2016).
[38] L. Zhao, R.A. Kerner, Z. Xiao, Y. L. Lin, K. M. Lee, J. Schwartz, and B. P. Rand, ACS Energy Lett. **1**, 3 (2016).
[39] X. Liu, C. Wang, L. Lyu, C. Wang, Z. Xiao, C. Bi, J. Huang, and Y. Gao, Phys. Chem. Chem. Phys. **17**, 2 (2015).
[40] Y. Yamada, T. Nakamura, M. Endo, A. Wakamiya, and Y. Kanemitsu, Appl. Phys. Express **7**, 3 (2014).
[41] P. Schulz, E. Edri, S. Kirmayer, G. Hodes, D. Cahen, and A. Kahn, Energy Environ. Sci. **7**, 4 (2014).
[42] H. Zhou, Q. Chen, G. Li, S. Luo, T. B. Song, H. S. Duan, Z. Hong, J. You, Y. Liu, and Y. Yang, Science **345**, 6196 (2014).
[43] N. Arora, M. I. Dar, A. Hinderhofer, N. Pellet, F. Schreiber, S. M. Zakeeruddin, and M. Grätzel, Science **358**, 6364 (2017).

DOI:10.1063/1674-0068/cjcp1808189